

# The Travelling Cluster Approximation for Strong Correlation Models of Lattice Fermions Coupled to Classical Fields

Sanjeev Kumar and Pinaki Majumdar  
*Harish-Chandra Research Institute,*  
*Chhatnag Road, Jhusi, Allahabad 211 019, India*  
 (June 3, 2004)

We suggest and implement a new Monte Carlo strategy for correlated models involving fermions strongly coupled to classical degrees of freedom, with accurate handling of quenched disorder as well. Current methods iteratively diagonalise the full Hamiltonian for a system of  $N$  sites with computation time  $\tau_N \sim N^4$ . This limits achievable sizes to  $N \sim 100$ . In our method the energy cost of a Monte Carlo update is computed from the Hamiltonian of a cluster, of size  $N_c$ , constructed around the reference site, and embedded in the larger system. As MC steps sweep over the system, the cluster Hamiltonian also moves, being reconstructed at each site where an update is attempted. In this method  $\tau_{N,N_c} \sim NN_c^3$ . Our results are obviously exact when  $N_c = N$ , and converge quickly to this asymptote with increasing  $N_c$ . The accuracy improves in systems where the effective disorder seen by the fermions is large. We provide results of preliminary calculations on the Holstein model and the Double Exchange model. The ‘locality’ of the energy cost, as evidenced by our results, suggests that several important but inaccessible problems can now be handled with control.

## I. INTRODUCTION

The equilibrium physics of classical interacting systems is by now very well understood. Quantum many body problems, involving strong interactions, however, remain difficult to solve with control. The focus of strong correlation theory is on devising methods to handle these problems. Techniques like density matrix renormalisation group<sup>1</sup> (DMRG) and dynamical mean field theory<sup>2</sup> (DMFT), for example, represent an advance in this direction. Problems where fermions are coupled to ‘classical fields’, *e.g.* large  $S$  spins, or ‘adiabatic’ phonons, are at an intermediate level of difficulty between purely classical systems and quantum many body problems. The quantum degrees of freedom are not directly interacting, so the difficulty with an exponentially growing Hilbert space is absent, but “annealing” the classical variables is much more difficult compared to purely classical systems.

The adiabatic approximation, whereby some degrees of freedom are treated as classical, is not novel. Several problems have been solved in the past by making this approximation, *e.g.* in electron-phonon systems<sup>3</sup>, or, in a different context, in the Car-Parrinello method<sup>4</sup>, handling coupled electronic and ionic degrees of freedom. The recent interest lies in the application of this approach to several strong coupling lattice fermion models, and some degree of success in understanding complex materials. Millis and coworkers<sup>5</sup> studied electrons coupled to classical spin and lattice (‘phonon’) degrees of freedom, to construct an initial theory of the manganites using DMFT. The approach was taken much farther by Dagotto and coworkers<sup>6</sup> using ‘real space’ Monte Carlo techniques to study ordering phenomena, phase coexistence, and disorder effects in a large family of correlation models pertinent to the manganites. The method has

been used extensively also to explore magnetism in double exchange (DE) based models<sup>7</sup>. For diluted magnetic semiconductors (DMS) too much of the physics has been clarified by methods which treat the doped magnetic moment as classical<sup>8</sup>. We ourselves have used the approach to study magnetism, insulator-metal transitions and nanoscale phase coexistence in disordered correlated electron models<sup>9,10</sup>.

The adiabatic limit simplifies the many body problem by casting it in the form of “non interacting” fermions in the background of classical variables,  $\{x\}$  say, but determining the distribution  $P\{x\}$  involves an expensive computation. In the absence of any small parameter to simplify the problem, computing  $P\{x\}$  requires iterative diagonalisation<sup>11</sup> of the fermion Hamiltonian and, for an  $N$  site system, the computation time,  $\tau_N$ , increases as  $N^4$ . We will describe the standard exact diagonalisation based Monte Carlo (ED-MC) in the next section, here we just note that the accessible sizes,  $N \sim 100$ , within ED-MC, severely limits the ability of the method to resolve the outstanding issues relating to transport, metal-insulator transitions, and the effect of disorder in correlated systems.

There have been some attempts at overcoming the severe finite size constraint in ED-MC. (i) Instead of exact diagonalisation, it has been proposed that the energy of fermions in the classical background can be estimated by moment expansion of the density of states. This, in principle, allows access to  $N \gtrsim 10^3$ , and has been used to study the clean<sup>12</sup> and disordered<sup>13</sup> DE model. (ii) A ‘hybrid’ Monte Carlo method, using dynamical evolution of the classical variables, has been tried out<sup>14</sup> for a model of competing DE and superexchange. (iii) We have proposed a scheme<sup>15</sup>, in the context of double exchange, where the energy associated with the spin configuration can be approximated by an *explicit* classical Hamiltonian

with couplings determined from a solution of the fermion problem.

While the approximations above have allowed some advance in the context of double exchange, there is no equivalent method available for handling phonon degrees of freedom, or the combination of phonons and spins (as relevant to manganites), or dilute strong coupling systems like the DMS. There is the need for a *general and computationally transparent method* that can handle models with arbitrary coupling and disorder, and systematically approach the ‘exact’ answer. This paper proposes such a scheme. We employ a variant of the exact diagonalisation strategy using an embedded (travelling) cluster, that estimates the energy cost of a Monte Carlo move by diagonalising the smaller cluster rather than the full Hamiltonian. Since size limitations are most severe in three dimension (3d), and it is physically also the most relevant, we benchmark our method directly in 3d, where the test is most stringent.

We will study two models, in 3d, to provide some performance benchmarks on the travelling cluster approximation (TCA). These are (i) the (disordered) Holstein model, and (ii) the double exchange model. They are, respectively:

$$\begin{aligned} H_1 &= -t \sum_{\langle ij \rangle} c_i^\dagger c_j + \sum_i (\epsilon_i - \mu) n_i - \lambda \sum_i n_i x_i + H_K \\ H_2 &= -t \sum_{\langle ij \rangle, \sigma} c_{i\sigma}^\dagger c_{j\sigma} + \sum_i (\epsilon_i - \mu) n_i - J_H \sum_i \mathbf{S}_i \cdot \hat{\sigma}_i \end{aligned} \quad (1)$$

The  $t$  are nearest neighbour hopping on a three dimensional lattice. In  $H_1$ , the on site binary disorder  $\epsilon_i$  assumes value  $\pm\Delta$ ,  $\mu$  is the chemical potential and  $n_i = c_i^\dagger c_i$  is the electron density operator (for spinless fermions), coupling to the phonon coordinate  $x_i$ .  $H_K = (K/2) \sum_i x_i^2$  where  $K = 1$  is the stiffness of the phononic oscillators. In  $H_2$ ,  $J_H$  is the Hunds coupling. The model is defined with ‘spinfull’ fermions, but since we will use  $J_H/t \rightarrow \infty$  it will also lead to an effective spinless fermion problem. We set  $t = 1$ , fixing our basic energy scale, and also  $\hbar = 1$ .

## II. METHOD

Let us start with the  $T = 0$  case to clarify the usual approach to these problems. Since we have earlier discussed the ED-MC method in detail<sup>15</sup> we only provide a brief outline here. There are several applications of ED-MC in the context of manganite related models<sup>11</sup>.

There are two (related) difficulties in solving strong coupling adiabatic problems. (i) The probability of occurrence of a classical configuration is not explicitly known, and is governed by the fermion free energy. Generating these configurations involves the  $N^4$  cost specified earlier. Let us call this the ‘annealing problem’. (ii) Even for a specified classical configuration, obtained

via some annealing technique, the electronic properties, *e.g.* the resistivity, involves computing fermionic correlation functions in a non trivial background. Since there is no analytic theory for non interacting fermions in an arbitrary ‘landscape’, transport calculations have to implement the Kubo formulae exactly. Our innovation in this paper is on the annealing problem, we still depend on a numerical implementation of linear response theory<sup>15</sup> to solve the transport problem on large lattices.

Let us start with the annealing problem. If we are at  $T = 0$ , the background in which the fermions move can be determined by minimising the total energy  $\langle H \rangle$  with respect to the classical variables. Denote the classical configuration as  $\{\eta_1, \eta_2, \dots\} \equiv \{\eta\}$ , where  $\eta_i = \eta(\mathbf{R}_i)$  and, in case of multiple classical variables at each site,  $\eta_i$  represents the full set of variables  $x_i, \mathbf{S}_i$ , etc, at that site. The key task is to determine  $\langle H \rangle = \mathcal{E}\{\eta\}$ .

If the coupling between the classical and quantum variables is *large*, there is no perturbative result for the fermion energy  $\mathcal{E}\{\eta\}$ , and therefore no explicit functional that we can minimise. This is where MC is used. The exact diagonalisation based method uses the following strategy: (i) Set up an arbitrary configuration  $\{\eta\}$  and compute the energy  $\mathcal{E}\{\eta\}$ . The fermion contribution is estimated by direct diagonalisation while the classical contribution,  $Kx_i^2$  say, is explicit. (ii) Attempt an update, say at site  $\mathbf{R}_i$ , by changing  $\eta_i \rightarrow \eta'_i$ . Compute the energy  $\mathcal{E}\{\eta'\}$ . (iii) If  $\Delta\mathcal{E} = \mathcal{E}\{\eta'\} - \mathcal{E}\{\eta\} < 0$ , accept the move, if  $\Delta\mathcal{E} > 0$ , and  $T \neq 0$ , accept the move with probability  $\propto e^{-\Delta\mathcal{E}/T}$ . (iv) Sweep over the system, initially to reach equilibrium and then to compute thermal averages.

The method above is simply a use of the Metropolis algorithm, with the complication of an expensive diagonalisation for every microscopic update. Since each local update involves computational effort  $\sim N^3$ , the cost of sweeping over the system leads to  $\tau_N \sim N^4$ . One has to multiply this with the cost of thermal averaging, and disorder average (if needed).

We were motivated to ask if it is really necessary to diagonalise the full Hamiltonian of the  $N = L^3$  system to estimate the cost,  $\Delta\mathcal{E}$ , of a local move. Imagine a ‘large’ system, (with  $L = 20$ , say, for arguments sake) and some degree of ‘disorder’ seen by the electrons arising from the classical thermal fluctuations or quenched disorder. Qualitatively, if the effect of a change,  $\eta_i \rightarrow \eta'_i$ , does not ‘propagate’ very far, as one would expect in a system with some disorder, then the energy cost of the move should be calculable from a Hamiltonian which involves only electronic degrees of freedom in the ‘vicinity’ of  $\mathbf{R}_i$ . We will discuss the analytic basis of such an argument separately, for the Monte Carlo it only requires that we modify step (ii) of the ED-MC strategy, discussed earlier. We compute  $\Delta\mathcal{E}$  as  $\mathcal{E}_c\{\eta'\} - \mathcal{E}_c\{\eta\}$ , where  $\mathcal{E}_c\{\eta\}$  is the energy computed by constructing a Hamiltonian of  $N_c = L_c^3$  sites around  $\mathbf{R}_i$ , and diagonalising this Hamiltonian in the background configurations  $\{\eta\}_c$  and  $\{\eta'\}_c$ , where the curly brackets,  $\{\}_c$ , refer to the configuration within the

cluster. We will show results on ‘equilibration’ within the TCA approach in the last section.

After equilibration the fermion properties are computed by diagonalising the *full*  $L^3$  Hamiltonian in the equilibrium background. Transport properties are calculated based on the spectrum and states obtained from these diagonalisation, using the Kubo formula<sup>15</sup>.

### III. RESULTS

Apart from the electronic parameters, the two computational parameters in the problem are  $N$  and  $N_c$ . In our notation  $\text{TCA}(N : N_c)$  implies MC for a  $N$  site system based on a cluster of size  $N_c$ . ED-MC obviously corresponds to  $\text{TCA}(N : N)$ . We assume a cube geometry, with periodic boundary conditions (PBC) for both the system and the cluster. Ideally one should have  $\text{TCA}(N : N)$  available for large sizes and study convergence as  $N_c \rightarrow N$ . Unfortunately ED-MC can be done, with great effort, only for sizes  $\lesssim 6^3$ , so  $\text{TCA}(N : N)$  will be rarely available at large  $N$  and we have to analyse the approximation based on the following checks.

(1). We study  $H_1$  and  $H_2$  using ED-MC on the largest possible lattice,  $N = 6^3$ . With somewhat reduced thermal averaging, and using scan in  $T$  (at fixed electron density), or a scan in  $\mu$  (at fixed temperature), we establish the ‘large size’ exact results. We then use  $\text{TCA}(N : N_c)$  with  $N_c = 3^3, 4^3$  and  $5^3$  to check the convergence to  $\text{TCA}(N : N)$ .

(2). We study a ‘large’ system,  $N = 8^3$ , and monitor the trend in  $\text{TCA}(N : N_c)$  with growing  $N_c$ , remaining in the regime  $N_c \ll N$ . We use  $N_c = 3^3, 4^3, 5^3$  to assess the convergence of the results to an asymptote with  $N_c$  still  $\ll N$ .

(3). We compare the energy cost of actual microscopic MC updates between ED-MC and TCA. We evolve a system via  $\text{TCA}(8^3 : 4^3)$  but simultaneously compute the energy cost of the updates via exact diagonalisation of the full  $8^3$  system. This is done by choosing a site randomly and computing both the exact  $8^3$  energy cost and the  $L_c^3$  energy cost whenever an update is attempted at that site. This yields information on how well TCA *microscopically* estimates the energy cost, rather than at the level of system averaged properties.

#### A. Clean Holstein Model

The Holstein model provides the minimal description of coupled electron and phonon degrees of freedom and, in the adiabatic limit, involves the following phases<sup>16–18</sup>, (i) a Fermi liquid (FL) metal, without any lattice distortions at  $T = 0$ , (ii) a positionally disordered insulating polaron liquid (PL) at strong coupling, and (iii) charge

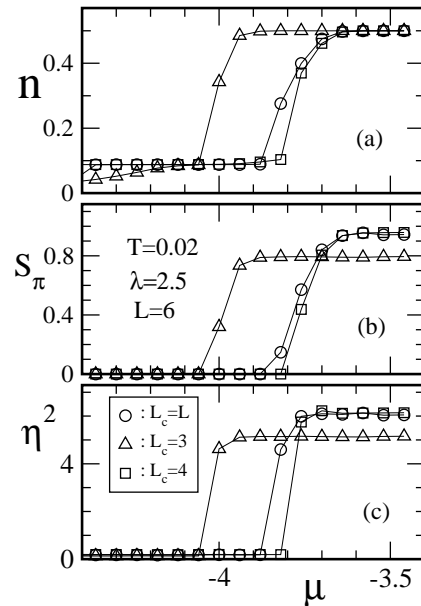


FIG. 1. The result of  $\mu$  variation in the clean Holstein model at coupling  $\lambda = 2.5$  and  $T = 0.02$ . The exact result, with  $L = 6$ , is compared to results with  $L_c = 3$  and  $L_c = 4$ . Panel (a). the variation in electron density, showing the discontinuous jump from the Fermi liquid to a charge ordered state, (b). the variation in charge order parameter with  $\mu$ , and (c). the variance of the effective disorder (see text) seen by the electrons. We have not used  $L_c = 5$  since the results on  $L_c = 4$  are already very close to ED with  $6^3$ .

ordered insulating (COI) phases close to  $n = 0.5$ . The physics of these phases has been discussed earlier within DMFT, and we also discuss it in detail in separate papers<sup>20,21</sup>. Our intention here is to estimate the effectiveness of TCA in capturing the known features of the Holstein model as well as compare with exact MC calculations.

Fig.1 and Fig.2 show the variation in carrier density,  $n(\mu)$ , the order parameter  $S(\pi, \pi, \pi)$  for commensurate charge ordering, and the variance of the ‘effective disorder’,  $\eta^2$  (defined further on), seen by the electrons, with varying  $\mu$  at two temperatures. In a model which has the possibility of phase separation, and ‘disallows’ a certain density range, it is imperative to work with constant  $\mu$  to map out the phase diagram. At the specified  $T$  and  $\mu$ , TCA is used to obtain a family of equilibrium phonon configurations, which are then used to solve the full electron problem.

Fig.1 pertains to low temperature,  $T = 0.02$ , at intermediate coupling, where there are two phases, (i) a FL at low doping,  $n \lesssim 0.1$ , and (ii) a commensurate COI phase for  $0.35 \lesssim n \lesssim 0.5$ , and a regime of phase separation for  $n$  between  $\sim 0.1 - 0.35$ . Before analysing the size dependence of the TCA results let us define the basic indicators. Fig.1.(a) shows  $n(\mu)$ , including the ‘discontinuity’ due to phase separation. Fig.1.(b) shows the COI order parameter  $S(\pi, \pi, \pi)$ , computed from the structure factor  $S(\mathbf{q}) = (1/N^2) \sum_{ij} \langle n_i \rangle \langle n_j \rangle e^{i\mathbf{q} \cdot (\mathbf{R}_i - \mathbf{R}_j)}$ , where  $\langle n_i \rangle$

is the quantum average of  $n_i$  in a MC configuration and the outer angular brackets indicate average over configurations. Fig.1.(c) shows the effective disorder based on the following prescription: for the Holstein model the electrons see a potential  $\xi_i^\alpha = \epsilon_i - \lambda x_i^\alpha$ , where  $\epsilon_i$  is the extrinsic disorder and  $x_i^\alpha$  is the structural distortion in an equilibrium MC configuration ( $\alpha$  is a MC configuration index). A crude measure of the ‘disorder’ seen by the electrons is provided by the variance of the  $\xi_i$  distribution, averaged spatially and over MC configurations. If we denote  $\eta_i = \xi_i - \bar{\xi}$ , where  $\bar{\xi}$  is the spatial average, then the effective disorder  $\eta^2 = \langle \eta_i^2 \rangle$ . It is the thermal and configuration averaged disorder that dictates the single particle scattering, and to some extent the transport properties. Our  $\eta^2$  data in Fig.1.(c), and later figures, quantify this disorder.

The data in Fig.1 and Fig.2 are on a  $6^3$  system, using clusters of  $3^3$ ,  $4^3$  and  $6^3$  itself to anneal the  $\{x_i\}$ . Comparing the cluster size dependence of the various physical quantities it is obvious that while updating using the  $3^3$  cluster is unable to accurately capture the effects in the  $6^3$  system, the results based on  $4^3$  are qualitatively similar to that of  $6^3$ . The size difference between the cluster and the full system is a factor of  $6^3/4^3 \sim 3.4$ . The ratio of the computation time between ED-MC on  $6^3$  and TCA( $6^3 : 4^3$ ) is  $\sim 40$ , if the same extent of averaging is employed in both calculations.

At higher temperature,  $T = 0.08$ , Fig.2, the results based on  $3^3$  continue to differ from the exact  $6^3$  result but the  $4^3$  result is virtually indistinguishable from the

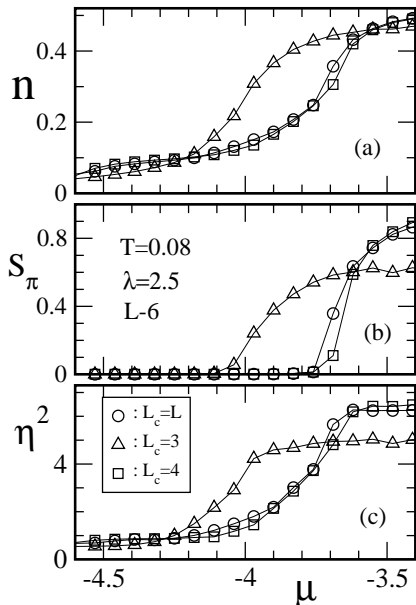


FIG. 2. Same as in Fig.1, except for  $T = 0.08$ . At this higher temperature the coexistence jump is almost smoothed out. The agreement between the exact result and TCA( $6^3 : 4^3$ ) is even better here.

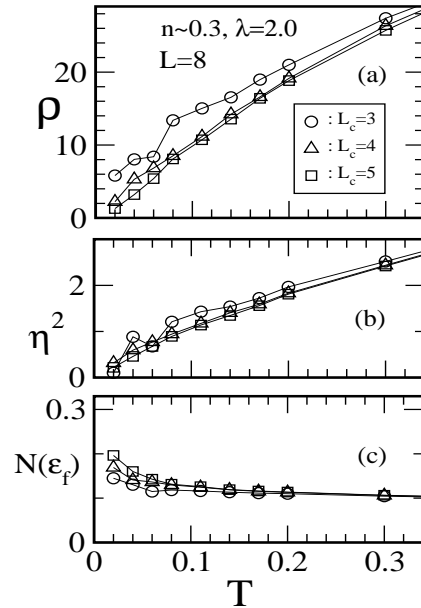


FIG. 3. Holstein model in the metallic regime,  $\lambda = 2.0$  and  $n = 0.3$ . Results with TCA( $8^3 : L_c^3$ ), with  $L_c = 3 - 5$ . Panel (a): resistivity  $\rho(T)$ . Except at the lowest  $T$ , the results with  $L_c = 4$  and  $L_c = 5$  are virtually indistinguishable, while  $L_c = 3$  matches the large cluster data only at high  $T$ . Panel (b): the effective disorder seen by the electrons, and panel (c) the density of states at the Fermi level.

exact answer. The key to this lies in the large damping of the electrons arising from thermal fluctuations, and at this temperature the effect of the  $4^3$  finite size gap is no longer relevant.

Fig.3 shows a different kind of result, where the system is studied via TCA at constant density,  $n = 0.3$ , at EP coupling  $\lambda = 2.0$ , on a “large” system,  $L = 8$ , with cluster size varying from  $3^3 - 5^3$ . We obviously cannot do an exact calculation on the  $8^3$  system, so the results in Fig.3 are intended to check out (i) the convergence of the TCA data to the  $N_c = N$  asymptote with growing  $N_c$ , and (ii) study the temperature dependence of this convergence, since strong disorder, *i.e.*, large  $\eta^2$ , at high temperature could make even the  $3^3$  based calculation viable. In Fig.3 we directly compute the resistivity, using a method described in an earlier paper<sup>15</sup>, as well as  $\eta^2$  and the density of states  $N(\epsilon_F)$  at the Fermi level.

Here again, the results based on  $4^3$  and  $5^3$  clusters are virtually indistinguishable except at the lowest temperature. The result based on  $3^3$  is visibly different from that on  $4^3 - 5^3$  at the lower temperatures, but converges to a common value for  $T \sim 0.3$ , by which  $\eta^2$  is quite large. The results on  $\eta^2$  itself and  $N(\epsilon_F)$  are quite similar for all  $L_c$  at all  $T$ , but the resistivity (which is a more stringent comparison) differentiates the changing character of the result with varying  $L_c$ . We would like to draw a general conclusion from these results, and back them up as we discuss the disordered Holstein model in the next section. If the single particle damping rate,  $\Gamma$ , arising out of  $\eta^2$  is comparable to the finite size gap,  $12t/L_c^3$ , in the clus-

ter than the specific finite size features of the cluster are smeared out and it mimics a ‘large’ system. So, *annealing the variables on the large system via TCA is effective if  $\Gamma \gg W/N_c$ , where  $W$  is the bare bandwidth of the system.* For a fixed  $T$  (and extrinsic disorder) this condition can be met by increasing  $L_c$ , while for a fixed  $L_c$  the accuracy increases as the net disorder (from thermal fluctuations and extrinsic disorder) increases.

To substantiate this claim, as well as check the ability of TCA to capture the ‘fingerprints’ associated with a specific disorder realisation, we next consider the disordered Holstein model.

### B. Disordered Holstein Model

The key feature of the Holstein model is the possibility of ‘self-trapping’, *i.e.*, polaron formation, when the EP coupling exceeds a certain threshold. The critical coupling for single polaron formation<sup>19</sup> in 3d is  $\lambda_c/t \sim 3.3$ , which implies that the polaron ‘binding energy’  $E_p^c = \lambda^2/(2K) \sim 5.44t$ . This would imply that at  $\lambda = 2$ , where  $E_p = 2t$  we should be far from any polaronic instability. This is indeed true in the absence of disorder and Fig.3, for example, shows that the response is metallic with  $d\rho/dT > 0$ . However, even weak disorder,  $\Delta = 0.6$ , has dramatic effect in the FL phase, see Fig.4. This figure presents results on the disordered Holstein model studied directly via ED-MC on  $6^3$ , as well as by TCA using  $3^3$  and  $4^3$  clusters on the  $6^3$  system.

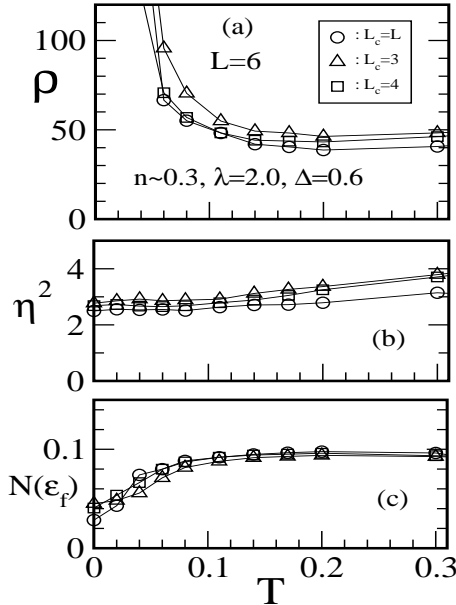


FIG. 4. Disordered Holstein:  $\lambda = 2.0$ ,  $\Delta = 0.6$ , and  $n = 0.3$ , exact results using  $6^3$  and TCA. TCA is based on  $L_c = 3$  and  $L_c = 4$ . Panel (a). resistivity  $\rho(T)$ , panel (b). the effective disorder  $\eta^2$ , panel (c). the density of states at the Fermi level.

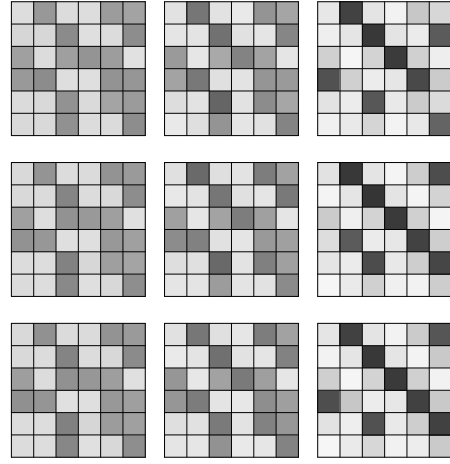


FIG. 5. Thermally averaged density profile, top surface of a  $6^3$  system: comparing exact results on  $6^3$  with TCA. The top row is for  $L_c = 3$ , next for  $L_c = 4$  and lowest for  $L_c = L = 6$ . Temperature, left to right, are 0.3, 0.11, 0.01. The disorder realisation  $\{\epsilon_i\}$  is the same in all cases.

In terms of the physical effect of disorder, the ED-MC indicates that the interplay of disorder and EP coupling can turn the system into a very bad metal (or even insulator) with a large resistivity at  $T = 0$ , and  $d\rho/dT < 0$  for  $T \rightarrow 0$ , Fig.4.(a). The ‘effective disorder’ seen by the electrons is large down to  $T = 0$ , Fig.4.(b), and there is a pseudogap in the DOS, as evident from  $N(\epsilon_F)$ , Fig.4.(c).

The conversion of a FL (at  $\lambda = 2.0, \Delta = 0$ ) into a ‘polaronic’ phase by weak disorder happens because the density inhomogeneity created by weak disorder is dramatically amplified by strong EP coupling<sup>21,22</sup> leading to strong localisation. However, all electronic states are not strongly localised, as the spatial pattern, Fig.5, and  $N(\epsilon_F)$ , Fig.4.(c), indicate. Fig.5, discussed further on, shows the thermally averaged density  $n_r$ .

In contrast to our results on the clean Holstein model, Fig.1-3, notice that *all* the sizes,  $3^3$ ,  $4^3$  and  $6^3$ , yield similar results on all the indicators, Fig.4.(a)-(c). While the  $4^3$  based results almost coincide with the exact  $6^3$  answer even the  $3^3$  based results capture all the qualitative features and even the numerical values reasonably accurately. The large effective disorder in the problem, arising from the strong lattice distortions,  $x_i$ , makes even the  $3^3$  calculation acceptable. The  $\eta^2$  in this model is  $\sim 3.0$  over the whole  $T$  range, comparable to the *maximum*  $\eta^2$  in the clean problem, Fig.3.(b).

While the transport and spectral properties seem to be adequately captured by TCA, does the method succeed in capturing the specific ‘fingerprint’ of a disorder realisation,  $\{\epsilon_i\}$ ? Fig.5 shows the thermally averaged density pattern,  $n_r$ , at three different temperatures (along the row) computed via TCA using  $L_c = 3$  (first row),  $L_c = 4$  (second row) and the exact,  $L_c = L = 6$  case (bottom row). The TCA was run with the *same realisation* of disorder in all three cases. Remember that while the cluster based update is used for the phonon degrees of freedom, the

final density field is calculated by diagonalising the *full Hamiltonian* in the background of the quenched disorder and the phonon configurations obtained via TCA. The cluster diagonalisation by itself cannot yield the density field.

At first glance, the results of all three runs, compared along a column, match well. At intermediate and high temperature there is weak but still visible density contrast and the results of all three schemes match very well. At the lowest temperature, the contrast is strongest and, although the correspondence along the third column is quite striking, there are some minor variations between the panels. This is partly because the MC based annealing is less effective at low temperature due to the small acceptance rate of moves. Apart from this generic difficulty with MC calculations, we think the overall ability of TCA to capture the specific features of a disorder realisation (and not just system averaged properties) is quite impressive.

Now consider using TCA on large sizes,  $L = 8$ , as in Fig.3, for the disordered problem. Fig.6 shows TCA based results using  $L_c = 3, 4, 5$  to solve the  $L = 8$  problem, and Fig.7 shows the associated density profile. As stated before it is impossible to do ED-MC on  $8^3$ , so the data here is meant to indicate the convergence of the TCA based results to the  $N_c \rightarrow N$  asymptote, although the exact result at  $N_c = N$  is not available. The effective disorder, Fig.6.(b), and  $N(\epsilon_F)$ , Fig.6.(c), are very similar for all  $L_c$ , and even the resistivity, Fig.6.(a), matches quite well after disorder average over  $\sim 4 - 5$  copies.

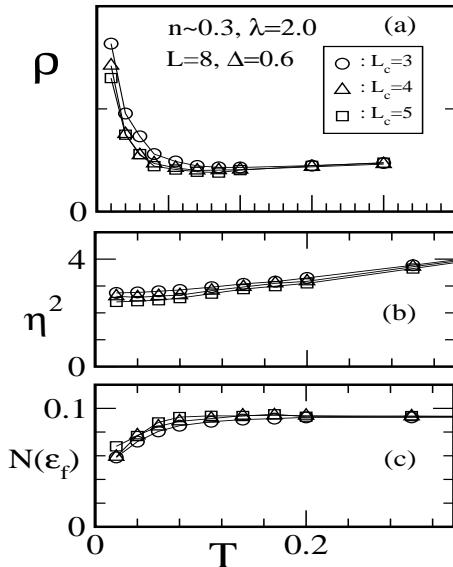


FIG. 6. Disordered Holstein model,  $\lambda = 2.0$  and  $n = 0.3$ ,  $\Delta = 0.6$ . Results with TCA ( $8^3 : L_c^3$ ), with  $L_c = 3 - 5$ . Panel (a): resistivity  $\rho(T)$ , (b): the effective disorder seen by the electrons, and (c) the density of states at the Fermi level.

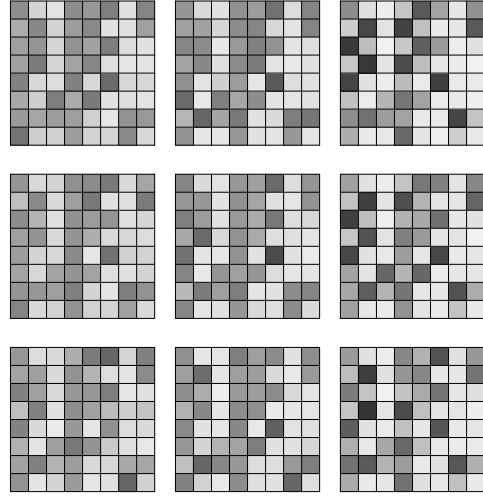


FIG. 7. Thermally averaged density profile: comparing TCA based results on a  $8^3$  system using  $L_c = 3, 4, 5$ . The top row is for  $L_c = 3$ , next for  $L_c = 4$  and lowest for  $L_c = L = 5$ . Temperature, left to right, are 0.4, 0.14, 0.04. The disorder realisation  $\{\epsilon_i\}$  is the same in all cases.

We would argue that for the conditions studied, TCA with  $L_c = 3 - 5$  is quite adequate in annealing the phonon variables on  $L = 8$ . *In fact when  $L_c$  is large enough, so that  $\Gamma \gtrsim 12t/L_c^3$ , the outer limit, i.e. system size  $L$ , is actually irrelevant.* Updates based on small clusters can successfully generate the appropriate configurations on large lattices. The only reason large  $L$  is needed at all, for the system as a whole, is to compute transport properties, or check for long range order.

The thermally averaged density profile corresponding to the MC in Fig.6 are shown in Fig.7. As in Fig.5, the patterns along each row correspond to decreasing  $T$ , reducing from  $T = 0.4$  to 0.14 to 0.04. The first row corresponds to TCA with  $L_c = 3$ , the second with  $L_c = 4$  and the third to  $L_c = 5$ . All three systems have the same realisation of quenched disorder  $\{\epsilon_i\}$ . Again, as in Fig.5, the different TCA results are in excellent agreement at higher temperature (first two columns) while there are some differences at the lowest temperature due to the difficulty in annealing. The actual percent difference in the density field, between the three systems, averaged over the whole  $8^3$  system is  $\sim 10 - 15\%$ .

### C. Double Exchange Model

The clean double exchange model has been widely studied, using a variety of analytical approximations and numerical techniques. We do not enter into a detailed recapitulation of these results since we have already reviewed them in detail<sup>15</sup> in an earlier paper. Here we focus primarily on MC based results, since these are unbiased, although necessarily finite size. The ground state of the clean DE model is a saturated ferromagnet and in terms

of transport both the ferromagnetic and paramagnetic phase are metallic.

In the limit  $J_H/t \rightarrow \infty$  the DE model maps on to a spinless fermion problem, with ‘hopping disorder’ arising from the background spin configuration. Since the strong local coupling  $J_H$  couples the core spin orientation to fermion spin projection, only the ‘locally aligned’ fermion state is viable at each site (the other is at an energy  $J_H$  above). The electron *hopping* between two sites depends on the electronic eigenfunctions at each site, and so on the spin orientation. The ‘projected’ Hamiltonian<sup>15</sup> turns out to be:

$$\begin{aligned} H &= -t \sum_{\langle ij \rangle} (g_{ij} \gamma_i^\dagger \gamma_j + h.c.) - \mu \sum_i n_i \\ &= -t \sum_{\langle ij \rangle} f_{ij} (e^{i\Phi_{ij}} \gamma_i^\dagger \gamma_j + h.c.) - \mu \sum_i n_i \end{aligned} \quad (2)$$

The  $\gamma$ ’s are spinless fermion operators. The hopping amplitude  $g_{ij} = f_{ij} e^{i\Phi_{ij}}$  between locally aligned states, can be written in terms of the polar angle ( $\theta_i$ ) and azimuthal angle ( $\phi_i$ ) of the spin  $\mathbf{S}_i$  as,  $\cos \frac{\theta_i}{2} \cos \frac{\theta_j}{2} + \sin \frac{\theta_i}{2} \sin \frac{\theta_j}{2} e^{-i(\phi_i - \phi_j)}$ . It is easily checked that the ‘magnitude’ of the overlap,  $f_{ij} = \sqrt{(1 + \mathbf{S}_i \cdot \mathbf{S}_j)/2}$ , while the phase is specified by  $\tan \Phi_{ij} = \text{Im}(g_{ij})/\text{Re}(g_{ij})$ .

Fig.8 shows MC results on the DE model, using  $L_c = 4$  and varying the system size from  $L = 4$  to  $L = 10$ . This is unlike our earlier results on the Holstein model where we kept the system size fixed and varied  $L_c$ , looking for convergence. For the DE model, there is already MC data available<sup>12</sup> on large sizes. Fig.8 shows the evolution of the magnetisation profile  $m(T)$  as  $L$  increases.

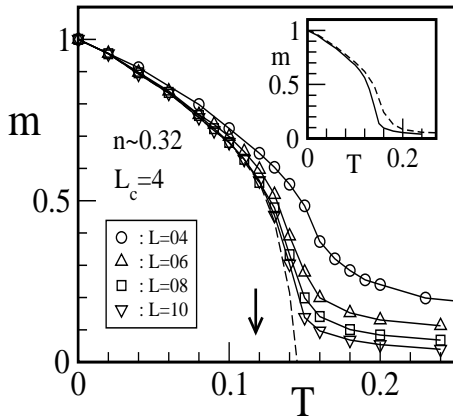


FIG. 8. Magnetisation in the clean DE model with  $L_c = 4$ , and  $L = 4 - 10$ . The electron density is  $n = 0.32$ . The magnetisation profile obtained by extrapolation to  $L \rightarrow \infty$  is shown as a dotted line. The arrow indicates  $T_c$  using the the moment expansion based MC and finite size scaling by Furukawa *et al.*. The inset compares the TCA result to an earlier ‘effective Hamiltonian’ approximation made by us.

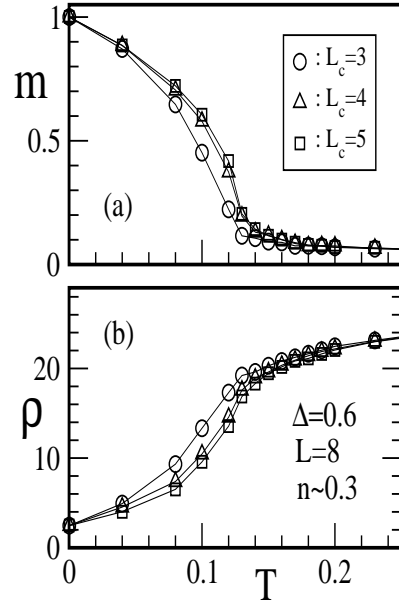


FIG. 9. Disordered DE model: magnetisation and resistivity. with  $L_c = 3, 4, 5$ , and  $L = 8$ . The electron density is  $n = 0.30$ .

The large  $L$  extrapolation of this trend, at  $L_c = 4$ , suggests  $T_c \approx 0.14$ . The result of moment expansion based MC and finite size scaling<sup>12</sup> indicate  $T_c \approx 0.12$  at this density. Although there is a difference between these results, the ability of TCA to approach the exact answer, with substantially less computational effort, is evident. The inset in Fig.8 compares an earlier approximation used by us<sup>15</sup> (using a classical effective Hamiltonian for the spins) with the TCA using  $L = 10, L_c = 4$ . The improvement in TCA, particularly in capturing the  $T_c$  scale is obvious.

Fig.9 shows results on the DE model in the presence of weak disorder in the electron system. This model has an additional term  $\sum_i \epsilon_i n_i$  where the  $\epsilon_i$  is binary disorder with strength  $\pm \Delta$  as in the Holstein problem. The data on magnetisation and resistivity in Fig.9 is shown for  $N = 8^3$ , with  $L_c = 3, 4, 5$ . As in the Holstein problem, the profiles with  $L_c = 4$  and  $L_c = 5$  are barely distinguishable.

## D. Computational indicators

### 1. Equilibration

Since the TCA based MC does not compute the total energy of the system in the process of updating, unlike ED-MC, the process of equilibration and stability of the energy is not obvious. To explicitly confirm the nature of equilibrium fluctuations (and the absence of drift in the mean value) as well as visualise the process of equilibration in response to a temperature step, we ran TCA with a simultaneous calculation of the total energy at the end of each MC sweep. The results, for the Holstein model,

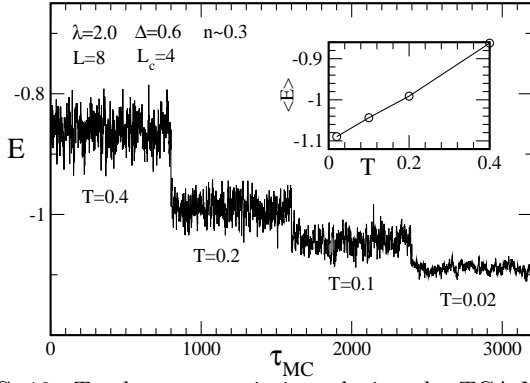


FIG. 10. Total energy variations during the TCA-MC on the Holstein model. The electronic parameters and temperatures are marked on the Figure. This trace is quite similar to that obtained in a typical ED-MC run, and the energy fluctuations reduce as expected with decreasing temperature. The inset shows the thermally averaged energy at each  $T$  as a function of temperature.

are shown in Fig.10. Notice that this requires diagonalisation of the full Hamiltonian matrix  $N_{MC}$  times, rather than  $N_{MC}N$  times as required by ED-MC. Apart from assurance about proper equilibration this diagnostic allows us to track potential hysteresis effects, *i.e.*, difference between heating and cooling, if a first order transition is involved.

## 2. Comparing $\Delta\mathcal{E}$

It may be useful to check out the claim that *microscopically* the TCA based calculation of  $\Delta\mathcal{E}$  quickly converges with increasing  $N_c$  (even if it is still  $\ll N$ ) and with increasing extrinsic disorder. To that effect Fig.11 analyses the results on the Holstein model. We update the system using TCA with  $L_c = 3 - 5$  on a  $L = 8$  system. For each  $L_c$ , and specified  $T$ , we choose a reference site randomly, and whenever a phonon update is attempted at that site in the course of the MC sweep, we not only compute the cluster based energy difference  $\Delta\mathcal{E}_c$  but also the *exact* energy cost of such a move  $\Delta\mathcal{E}_{ED}$  based on the full system.

The system evolves according to TCA, but we keep track of these energy differences (at that site) and construct the following error measure:

$$\delta(L_c, L) = \frac{1}{N_{MC}} \left| \frac{\Delta\mathcal{E}_c - \Delta\mathcal{E}_{ED}}{\Delta\mathcal{E}_{ED}} \right| \quad (3)$$

where the averaging is over MC steps, and the ‘error’  $\delta$  implicitly depends on temperature, as well as all other electronic parameters (in particular, disorder).

Fig.11 shows results, again on the Holstein model, with  $L = 8$  and  $L_c = 4$ , panel (a). The state at  $T = 0$  is a *clean Fermi liquid* for  $T = 0$ , the electronic states are simple tight-binding states and, as expected,  $\Delta\mathcal{E}$  computed on  $8^3$  and  $4^3$  have a fair difference, about 25%. This “error”

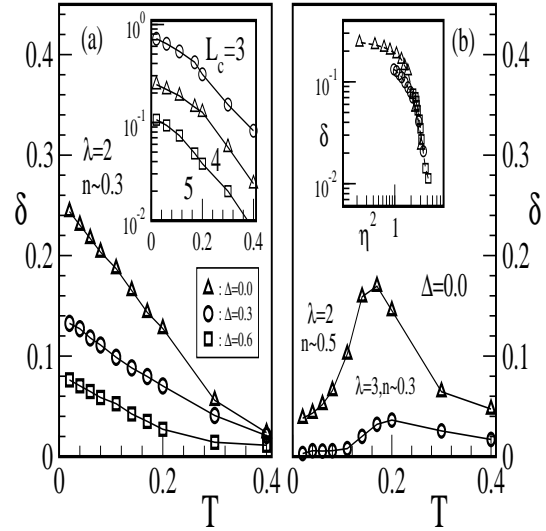


FIG. 11. Error in energy estimate of MC moves. The indicator  $\delta$  defined in the text, compares energy costs on the full  $L^3$  system with that based on  $L_c^3$  clusters. Panel (a) shows the  $T$  dependence of  $\delta$  with increasing disorder, and the inset shows the  $L_c$  dependence at  $\Delta = 0$ . Panel (b) same as in panel (a) with different parameters, marked on the Figure. Inset to panel (b) variation of  $\delta$  with the effective disorder,  $\eta^2$ , combining the results in main panel (a).

falls quickly with increasing temperature, as thermal fluctuations in the  $x_i$  increase (staying at  $\Delta = 0$ ), and also reduces systematically on introduction of even weak disorder  $\Delta = 0.3 - 0.6$ . The inset to Fig.11.(a) shows temperature dependence of the error with varying  $L_c$  at  $\Delta = 0$ . To construct an approximate measure, the typical error, averaged over the temperature window is  $\sim 0.5$  at  $L_c = 3$ ,  $\sim 0.1$  at  $L_c = 4$ , and  $\sim 0.05$  at  $L_c = 5$ . Fig.11.(b) shows  $\delta$  at  $n = 0.5, \lambda = 2.0$  (which is a charge ordered state at low temperature) and  $n = 0.3, \lambda = 3.0$  (which is a polaronic insulator) again at  $L = 8$  with  $L_c = 4$ . The error in the CO problem is non monotonic because, unlike the Fermi liquid, the system goes into a ordered chessboard phase at  $T = 0$  and this localisation reduces the error. In the polaronic insulator phase the error is below the 5% threshold at all temperatures due to the strongly localised nature of electronic wavefunctions. The inset to Fig.11.(b) puts together the error variation with respect to the effective disorder,  $\eta^2$ , for the data in Fig.11.(a) for  $\Delta = 0 - 0.6$  with varying temperature. As we have argued earlier there is a roughly ‘universal’ behaviour of the error in terms of the effective disorder, *irrespective of its origin*, and at  $L_c = 4$  an error  $\lesssim 0.1$  is obtained whenever  $\eta^2 \gtrsim 1.0$ .

Note that  $\delta$  above is a measure of error in the energy estimate, we have checked that the error in  $e^{-\beta\Delta\mathcal{E}}$  itself, which controls the MC moves, between the  $4^3$  and  $8^3$  cluster are much smaller than the error in  $\Delta\mathcal{E}$ . This explains why the thermodynamic and transport results are accurate even with  $L_c = 4$  in the clean system.



#### IV. CONCLUSION

Since we have put forward the TCA based approach to adiabatic problems as a ‘general’ many body technique, not restricted to the specific examples studied here, let us compare it with DMFT<sup>2</sup> which finds wide use as a method for handling correlated electrons. (i) DMFT maps on a correlated lattice problem to an impurity model, reducing it to an effective single site problem and making it more tractable. The adiabatic approach, and the TCA approximation, ignores the quantum dynamics of the background fields, leading to a static but ‘annealed’ disorder problem. (ii) The two methods have complementary reach. DMFT is good at handling local quantum correlations but misses out on spatial fluctuations and disorder physics. The real space adiabatic approach, supplemented by TCA like approximations, handles disorder and spatial correlations accurately but cannot handle interacting quantum modes. (iii) Both have had significant success in materials physics. DMFT extended to include non local correlations will be truly global method, the adiabatic approach extended to include quantum dynamics, and implemented via TCA like approximations, or refinements, would ‘reach’ real life problems from another direction.

In conclusion, we have put forward and benchmarked a new Monte Carlo technique for handling fermions strongly coupled to classical degrees of freedom. The method relies on the approximate ‘locality’ of the energy cost of a MC move in a system with moderate disorder, allowing accurate estimate of energy differences to be made using on a cluster Hamiltonian instead of the full system. This allows annealing of the classical variables on large lattices, breaking the  $N^4$  barrier that plagues exact diagonalisation based Monte Carlo. The approach makes no assumptions regarding the the starting Hamiltonian, except the quadratic nature of the quantum degrees of freedom. We have provided basic benchmarks on the Holstein and Double Exchange model, and will provide several new results in forthcoming papers.

We acknowledge use of the Beowulf cluster at HRI.

- <sup>5</sup> A. J. Millis, B. I. Shraiman, and R. Mueller, Phys. Rev. Lett. **77**, 175 (1996).
- <sup>6</sup> See *e.g.*, S. Yunoki, J. Hu, A. L. Malvezzi, A. Moreo, N. Furukawa, and E. Dagotto, Phys. Rev. Lett. **80**, 845 (1998), S. Yunoki, T. Hotta, and E. Dagotto, Phys. Rev. Lett. **84**, 3714 (2000).
- <sup>7</sup> M. J. Calderon and L. Brey, Phys. Rev. **B 58**, 3286 (1998), Y. Motome and N. Furukawa, J. Phys. Soc. Jpn. **68**, 3853 (1999).
- <sup>8</sup> G. Alvarez, M. Mayr, and E. Dagotto, Phys. Rev. Lett. **89**, 277202 (2002).
- <sup>9</sup> Sanjeev Kumar and Pinaki Majumdar, Phys. Rev. Lett. **91**, 246602-1 (2003).
- <sup>10</sup> Sanjeev Kumar and Pinaki Majumdar, Phys. Rev. Lett. **92**, 126602 (2004).
- <sup>11</sup> S. Yunoki, *et al.*, Phys. Rev. Lett. **80**, 845 (1998), E. Dagotto, *et al.*, Phys. Rev. **B 58**, 6414 (1998).
- <sup>12</sup> Yukitoshi Motome and Nobuo Furukawa, J. Phys. Soc. Jpn. **72**, 2126 (2003).
- <sup>13</sup> Y. Motome and N. Furukawa, J. Phys. Chem. Solids, **63**, 1357 (2002).
- <sup>14</sup> J. L. Alonso, L. A. Fernandez, F. Guinea, V. Laliena, V. Martin-Mayor, Nucl.Phys. **B 596**, (2001) 587-610
- <sup>15</sup> Sanjeev Kumar and Pinaki Majumdar, cond-mat 0305345.
- <sup>16</sup> A. J. Millis, R. Mueller, and B. I. Shraiman, Phys. Rev. **B 54**, 5389 (1996).
- <sup>17</sup> S. Ciuchi and F. de Pasquale, Phys. Rev. **B 59**, 5431 (1999).
- <sup>18</sup> S. Blawid and A. J. Millis, Phys. Rev. **B 62**, 2424 (2000).
- <sup>19</sup> See, *e.g.*, A. H. Romero, D. W. Brown and K. Lindenberg, Phys. Rev. **B 60**, 14080 (1999).
- <sup>20</sup> Sanjeev Kumar and Pinaki Majumdar, cond-mat 0406083.
- <sup>21</sup> Sanjeev Kumar and Pinaki Majumdar, cond-mat 0406084.
- <sup>22</sup> See, *e.g.*, D. Emin and M.-N. Bussac, Phys. Rev. **B 49**, 14290 (1994) for the interplay of *extrinsic* disorder and EP coupling.

---

<sup>1</sup> S. R. White, Phys. Rev. Lett. **69**, 2863 (1992), see Karen Hallberg, cond-mat 0303557, for a recent review.

<sup>2</sup> Antoine Georges, Gabriel Kotliar, Werner Krauth and Marcelo J. Rozenberg, Rev. Mod. Phys. **68**, 13 (1996). For recent reviews see, Tudor Stanescu and Gabriel Kotliar, cond-mat 0404722, Antoine Georges, cond-mat 0403123.

<sup>3</sup> A.B. Migdal, Sov. Phys. JETP **7**, 996 (1958), V.V. Kabanov and O.Y. Mashtakov, Phys. Rev. **B 47**, 6060 (1993).

<sup>4</sup> R. Car and M. Parrinello, Phys. Rev. Lett. **55**, 2471 (1985).